Realignment-enhanced coherent anti-Stokes Raman scattering and three-dimensional imaging in anisotropic fluids

Aliaksandr V. Kachynski[1], Andrey N. Kuzmin[1], Paras N. Prasad[1*], Ivan I. Smalyukh[2]**

#95590 - $15.00 USD Received 29 Apr 2008; revised 9 Jun 2008; accepted 11 Jun 2008; published 1 Jul 2008

#95590 - $15.00 USD Received 29 Apr 2008; revised 9 Jun 2008; accepted 11 Jun 2008; published 1 Jul 2008

42. Y. Fu, H. Wang, R. Shi, and J. -X. Cheng, "Characterization of photodamage in coherent anti-Stokes Raman scattering microscopy," Opt. Express **14**, 3942-3951 (2006).
43. H. Wang, Y. Fu, and J. X. Cheng, "Experimental observation and theoretical analysis of Raman resonance-enhanced photodamage in coherent anti-Stokes Raman scattering microscopy," J. Opt. Soc. Am. B **24**, 544-552 (2007).
44. I. I. Smalyukh, D. S. Kaputa, A. V. Kachynski, A. N. Kuzmin, and P. N. Prasad, "Optical trapping of director structures and defects in liquid crystals using laser tweezers," Opt. Express **15**, 4359-4371 (2007).
45. I. I. Smalyukh, "Confocal Microscopy of Director Structures in Strongly Confined and Composite Systems," Mol. Cryst. Liq. Cryst. **477**, 23-41 (2007).

1. Introduction

Raman scattering is at the core of many valuable optical spectroscopy and imaging techniques broadly used for characterization of materials and biological cells. This scattering is associated with specific frequencies of molecular vibrations and can provide information about chemical composition and structure of materials. However, spontaneous Raman scattering is a very weak optical effect that usually requires long signal integration times or/and high-power laser excitation beams, which sets the limits for many applications. The externally-stimulated coherent anti-Stokes Raman scattering (CARS, first demonstrated in 1965 by Maker and Terhune [1]) provides Raman signals 5-6 orders of magnitude stronger

microscope's optical axis) and averages out the information across the optical path of light in the LC sample. 3-D imaging of molecular orientations can be enabled by combining the complementary capabilities of PM and fluorescence confocal microscopy [20]; this approach, however, requires doping the LC with a specially-selected dye that has little or no influence on $\hat{n}$. The labeling-free confocal Raman microscopy with polarized excitation/detection [21, 22], that utilizes the spontaneous Raman signal dependence on orientations of molecular bonds, has also been recently applied to 3-D LC imaging; however, this technique requires long integration times of Raman signals and high excitation powers.

away from that of other most common chemical bonds typical for organic molecules (Fig. 1). The intensity is higher for orientation of the linear laser polarization parallel to $\hat{n}_0$ and the CN bonds and lower for the orthogonal one, Fig. 1, which is consistent with previous reports [37].

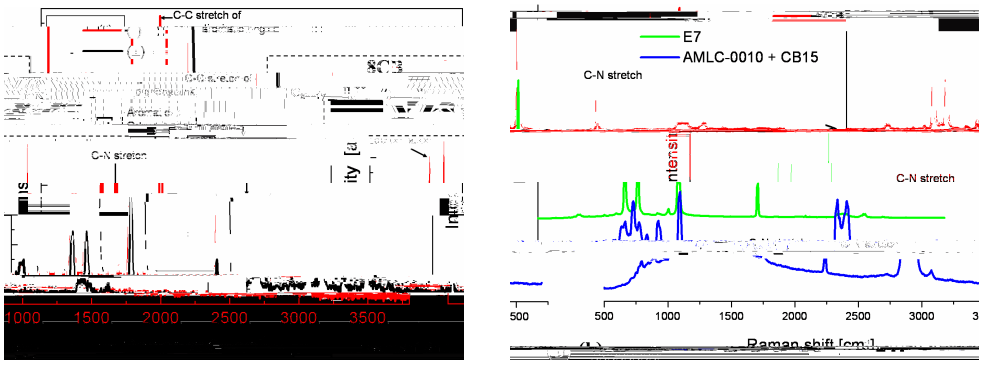

Fig. 1. Raman scattering spectra of the studied LC materials. (a) Raman scattering of 8CB for directions parallel and perpendicular to $\hat{n}_0$ in a planar cell; the inset shows chemical structure of the 8CB molecule. (b) Raman spectra for single-compound LC 5CB (red), nematic mixture E7 (green), and a mixture of nematic AMLC-0010 and chiral additive CB-15 (~1 Wt. %). For clarity, the spectra have been displaced with respect to each other along the "Intensity" axis.

2.2 CARS-PM setup

The simplified schematics of CARS-PM experimental set-up is shown in Fig. 2(a). A picosecond Nd:YVO4 (1064nm, picoTRAIN IC-10000, HighQ Laser) with the pulse width ~10 ps and a repetition rate of 76MHz is the source of the Stokes wave at ω_s and is also used to synchronously pump a tunable (780–920nm) intracavity-doubled periodically-poled crystal optical parametric oscillator (OPO, Levante from APE, Germany) with the output of ~10ps pulses. The synchronously pumped OPO coherent device provides temporal synchronization with the Nd:YVO4 and serves as a source of the pump/probe wave at $\omega_p = \omega_{pump} = \omega_{probe}$. The two picosecond laser beams are made coincident in time and in space with the help of a series of dichroic mirrors and are focused into a diffraction-limited volume in the sample using the objective lens, Fig. 2(a). CARS is a four-wave mixing process involving the pump/probe wave and the Stokes wave at frequencies ω_p and ω_s, respectively. When the beating frequency $\omega_p - \omega_s$ is tuned to be resonant with a given vibration mode of a selected chemical bond, an enhanced CARS signal is observed at the anti-Stokes frequency of $\omega_{as} = 2\omega_p - \omega_s$, Fig. 2(b). Using our setup, a sample can be imaged by utilizing vibration frequencies in the spectral range of $(1440 - 3400)cm^{-1}$. Six detection channels (two forward and four backward) allow us to record forward- and backward- propagated signals. Synchronously with the CARS signal, the system allows us to detect fluorescence (polarized two-photon fluorescence and confocal fluorescence microscopy modes), second and third harmonic generation signals, sum and difference frequency generation signals, etc. A computer-controlled XY galvano scanner (GSI Lumonics) scans the sample in the lateral focal plane of a water-immersion objective O1 (NA=1.2, UPLSAPO 60x, Olympus). Images are acquired by raster scanning as fast as 500000 pixels/s (signal integrd9ieeg2R i

(Hamamatsu). The M6 dichroic mirror and a series of narrow-bandpass barrier filters (F1) are used for spectral selection of F-CARS. Backward-detected CARS (E-CARS) in the reflection geometry is selected using the narrow-bandpass barrier filter F2. Polarizers P3 and P4 control the polarization states of the detected F-CARS and E-CARS signals, respectively; CARS experiments have been performed with parallel linear polarizations (denoted by $\hat{P}_{CARS}$) of the input Stokes and pump/probe beams as well as P3 and P4; the sample was rotated in order to change the angle between $\hat{P}_{CARS}$ and the LC director. The intensity of co-localized pump/probe and Stokes beams drops rapidly as one moves away from the focal plane. Thus, the nonlinear CARS signal is generated from a tiny submicron volume with highest excitation intensity and the sample can be imaged with a 3-D resolution by scanning the sample. The 3-D images are constructed from the series of XY scans (sample cross-sections) by software.

In addition to the CARS-PM mode described above, the setup allows for PM studies of the sample in the transmission mode, Fig. 2(a). A halogen lamp served as a light source; the light was passed through a set of mutually crossed polarizers P5 and P6, objectives O1 and O2 and the LC-sample, Fig. 2(a). The transmission PM mode of imaging allowed us to monitor the laser-induced reorientation during the excitation of CARS signal in the LC sample by using intense Stokes and pump/probe laser beams. In the Fluorescence Confocal Polarizing Microscopy (FCPM) imaging mode [20] (used for the control/comparison experiments), the BTBP dye (N,N'-Bis(2,5-di-tert-butylphenyl)-3,4,9,10-perylenedicarboximide, from Aldrich) was excited by an Ar-laser at 488*nm* and the polarized fluorescence signal was detected within the spectral range of (510-550)*nm*.

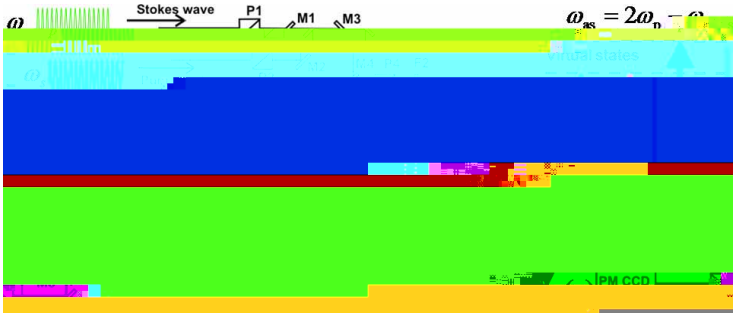

Fig. 2. CARS-PM setup and the principles of CARS imaging. (a) schematics of the experimental setup: ω_s and ω_p are frequencies of synchronized picosecond Stokes and

layers buffed to set the uniform in-plane far-field director $\hat{n}_0$, or with the polyimide JALS-204 (JSR, Japan) for the homeotropic surface anchoring ($\hat{n}_0$ perpendicular to the substrates); some of the samples were assembled using glass plates with transparent ITO electrodes needed for applying voltage. The LC sample thickness of $(5-40)\mu m$ was set using thin Mylar films placed along cell edges and then the cells were sealed using a UV-curable glue. To avoid any flow influence on the LC alignment, the LC cells were filled by the capillary forces in the isotropic phase and then slowly (~$0.1^0 C/min$) cooled down to the room temperature. After the material is brought into a nematic, cholesteric, or smectic phase, the studied defects and structures spontaneously nucleate and are studied with the CARS-PM technique.

3. Results

3.1 Angular dependencies of CARS intensity

Using the experimental CARS-PM setup shown in Fig. 2(a), we have tuned the input pump/probe frequency

pump/probe excitation beams, the simultaneously-measured E-CARS and F-CARS signals show similar angular dependencies, Fig. 4(b); the E-CARS signal is weaker (even at two-fold larger PMT gain) . Moreover, this dependence holds as ω_p is tuned away from the resonance condition (in our case to $\omega_p - \omega_s = 2284 cm^{-1}$), even though the detected Raman signal becomes several orders of magnitude weaker; we note that this is an expected result as the angular dependence of non-resonant signal (usually known as non-resonant background, or non-resonant electronic $\chi^{(3)}$ four-wave mixing signal [35,39]) displays similar behavior as that for the CARS signal in resonance. The strong angular dependence of the resonant I_{CARS} with the maximum at $\theta = 0$ allows one to decipher the director's spatial configuration based on a 3-D pattern of the measured CARS signal and makes CARS-PM a viable technique for mapping of the 3-D patterns of molecular orientations. Since the signal drops rapidly as θ departs from $\theta = 0$, CARS-PM visualizes $\hat{n}$ in the parts of a sample with maximum CARS intensity where $\hat{P}_{CARS} \| \hat{n}$. One of the advantages of CARS-PM as compared to FCPM is that $I_{CARS}(\theta)$ decreases much more rapidly as θ departs from $\theta = 0$ (corresponding to the maximum CARS signal) than in the case of $I_{FCPM}(\theta_{FCPM}) \propto \cos^4 \theta_{FCPM}$ (compare Fig. 4(a) with the angular dependence obtained in a control experiment for FCPM in Fig. 4(c)). Moreover, for $\theta = \pm(0-60)$ degrees, the experimental data agree well with the theoretical dependence of $I_{CARS}(\theta) \propto \cos^8 \theta$ [12], so that the image contrast in CARS-PM can be related to structures of $\hat{n}$ and the computer-

3.2

To address these aspects of CARS imaging that are specific solely to anisotropic fluids, we have explored the effects of director realignment on imaging of structures by using laser powers higher than usually needed for imaging of stationary director structures. We have varied the scanning area at constant high laser powers (Fig. 5(a)) as well as varied laser power

#95590 - $15.00 USD Received 29 Apr 2008; revised 9 Jun 2008; accepted 11 Jun 2008; published 1 Jul 2008

#95590 - $15.00 USD Received 29 Apr 2008; revised 9 Jun 2008; accepted 11 Jun 2008; published 1 Jul 2008

The 3-D configuration of the layers/director inside the FCD is rather complex. CARS-PM allows one to directly visualize the basic features of this director structure. Since the director field $\hat{n}(x, y, z)$

(such as the one in Fig. 9(c)), one reconstructs $\hat{n}(x, y, z)$ in the finger's vertical cross-section (Fig. 9(d)) based on the pattern of maximum intensity at spatial locations where $\hat{n}(x, y, z) \| \hat{P}_{CARS}$.

Fig. 10. (a-c) CARS-PM images of an array of axially-symmetric cholesteric domains obtained in a homeotropic cell with the AMLC-0010+CB15 mixture; the red ellipsoids on the inset show areas in which molecular orientations closely match orientation of $\hat{P}_{CARS}$ and correspond to high CARS intensity on the image. (d) schematics of the reconstructed $\hat{n}$ -structure in the domain.

By applying low-frequency electric field of $(20-200)Hz$ and $(5-20)V$ for 1min

Finally, we apply CARS imaging to visualize defect structures in the cholesteric layered system (Fig. 11) in the sample with planar boundary conditions where the cholesteric pitch $p \approx 5\mu m$ is much smaller than the cell thickness $d \approx 40\mu m$. Figure 11 shows two dislocations with Burgers vectors $|\vec{b}| = p$ of opposite signs (Fig. 11(b)) that combine to form the so-called Lehmann cluster of total Burgers vector equal to zero, Fig. 11(c). The dislocation cores in each case are split into the pairs of $\lambda^{+1/2}$ and $\lambda^{-1/2}$

excitation powers $W_p + W_S > 300mW$ that are two orders of magnitude higher than the threshold power for a stationary beam focused into a diffraction-limited spot in the same LC sample, Fig. 5. At the used scanning rates of ~500000pixels/s, the excitation and CARS signal integration time per pixel is more than three orders of magnitude shorter than the characteristic LC realignment time (10ms). Moreover, within the typical LC response time of 10ms, the CARS excitation beams can be scanned over the area 2-4 orders of magnitude larger than that of the diffraction-limited spot of the coincident excitation beams in CARS-PM ($\sim 1\mu m^2$). Thus, the effective threshold intensity of laser-induced realignment at such fast scanning rates increases according to the increase of the excitation area, Fig. 5, and nondestructive realignment-free imaging using high-power beams becomes possible. Since CARS intensity increases rapidly with increasing the excitation intensity, $I_{CARS} \propto I_{excitation}^3$, every two-fold increase of the excitation power will allow for 8-fold shorter signal integration times and, thus, strong CARS signals at fast scanning of high-power excitation beams [23]. This demonstrates the feasibility of nondestructive CARS-PM studies of dynamic processes in anisotropic fluids such as LCs, but only when high scanning rates are used.

Optics of the birefringent medium makes the CARS imaging of LCs more complicated than in the case of isotropic media and precautions are needed for avoiding of artifacts. In addition to the laser-induced realignment, CARS-PM imaging in anisotropic fluids may be accompanied by other artifact phenomena associated with light absorption and sample heating, influence of optical gradient forces acting on inclusions or director structures during the scanning [44, 45], light scattering due to director fluctuations [18], effects of birefringence (such as depolarization and defocusing of light) [20], laser beam's polarization following of the director twist (known as the Mauguin effect and adiabatic following of polarization [18]), chromatic aberrations resulting from the fact that the wavelengths of excitation beams and detected CARS are different, depolarization of linearly-polarized excitation beams due to focusing with high NA objectives, spherical and other aberrations, etc. In particular, by using objectives of different NA and LCs of different optical anisotropy, we find that the light depolarization due to the high NA objective and LC birefringence is responsible for the slight departure (within $\theta = 70-110$ degrees) of experimental angular dependence of CARS-PM intensity from the expected $I_{CARS}(\theta) \propto \cos^8\theta$, Fig. 4(a),(b). These artifacts do not compromise the capability of CARS-PM to visualize the LC director fields and can be minimized by the experiment and sample design, especially for the LCs with low optical anisotropy Δn (as tested using AMLC-0010 with $\Delta n \approx 0.075$ E7 with $\Delta n \approx 0.22$); detailed studies on these depolarization-related and other artifacts as well as approaches to mitigate them will be reported elsewhere.

5. Conclusions

We have demonstrated that the generation of CARS signal in anisotropic fluids such as liquid crystals can be accompanied by molecular and LC director realignment at high excitation laser intensities. These realignment effects can be avoided by limiting excitation powers or fast scanning and CARS polarization microscopy can visualize LC director structures, chemical composition, and bond/molecular orientation in anisotropic materials of technological imp.8(on)1u0013 Tcb'0.2(i)10.2(o0.3(u001(t)-3 Tcb'0.2(i)10.2(o0.3(u001(on93(n)1.4(t)-7.-16.9)] TJ)9.8(e1.2(n biot)-

Acknowledgments

This research was supported by the International Institute for Complex Adaptive Matter (I2CAM), the Directorate of Chemistry and Life Sciences of AFOSR, and the NSF Grant

#95590 - $15.00 USD Received 29 Apr 2008; revised 9 Jun 2008; accepted 11 Jun 2008; published 1 Jul 2008